---

**Article:**
Al Tannir, R., Pautrat, A., Soutrenon, R. et al. (2 more authors) (2025) Brainstem neuroadaptations in rodent models of Parkinson's disease. European Journal of Neuroscience, 61 (7). e70068. ISSN 0953-816X

https://doi.org/10.1111/ejn.70068

---

# Brainstem neuroadaptations in rodent models of Parkinson's disease

Al Tannir R[1], PhD, Pautrat A[1], PhD, Soutrenon R[1], Overton PG, PhD and Coizet V[1], PhD

**Author affiliations**:

1 Univ. Grenoble Alpes, Inserm, U1216, CHU Grenoble Alpes, Grenoble Institut Neurosciences, 38000 Grenoble, France

2 Department of Psychology, University of Sheffield, Sheffield, UK.

**Correspondance to**: Veronique Coizet

https://orcid.org/0000-0001-5192-6610

e-mail: veronique.coizet@univ-grenoble-alpes.fr

**Running title**: Brainstem in Parkinson's disease

**Keywords**: Parkinson's disease, Superior colliculus, Periaqueductal gray, Dendritic spines, $GABA_A$ receptors.

**Word counts**: 6651

**Figure count**: 4

**Table count**: 1

## LIST OF ABBREVIATIONS

AP: Antero-posterior

BSA: bovine serum albumin

DA: dopaminergic

DAB: 3,3'-diaminobenzidine

DV: dorso-ventral

IOD: integrated optical density

ML: medio-lateral

NHS: normal horse serum

OD: optical density

PAG: periaqueductal gray

PBN: parabrachial nucleus

PD: Parkinson's disease

PB: phosphate buffer

SC: superior colliculus

SDS: sodium dodecyl sulfate

SNc: substantia nigra pars compacta

SNr: Subtantia nigra pars reticulata

TH: tyrosine hydroxylase

TX: triton

6-OHDA: 6-hydroxydopamine

**Abstract**

A classical theory of a key pathophysiological change in Parkinson's disease (PD) is that GABAergic neurons in the substantia nigra pars reticulata (SNr), an output structure of the basal ganglia, become hyperactive following the dopaminergic loss. Increased GABA release from the SNr neurons is thus likely to induce neuro-adaptations in structures receiving a direct projection from the SNr, including the parabrachial nucleus (PBN), superior colliculus (SC) and periaqueductal gray (PAG). We have shown that the PBN indeed exhibits cellular and molecular changes in PD rat models. We thus expected the SC and the PAG to likewise show neuroplasticity. The objective of the present work was to evaluate the cellular and molecular plasticity in both the SC (lateral and medial) and the PAG in PD rats with a partial or total dopaminergic lesions. We used Golgi-Cox to measure the spine density and spine morphology, and Western blot to analyze $GABA_A$ receptor expression in both PD rat models compared to sham animals. We found an increase in spine density (thin and stubby types) following total dopaminergic lesions in the SC and the PAG. Additionally, increased $GABA_A$ receptor expression was observed in the lateral SC in the total lesion group only. These results suggest compensatory mechanisms in PD that may delay disease onset and contribute to both motor and non-motor symptoms. Further investigation should be performed to fully understand the functional impact of the plasticity revealed in this work.

## 1 | INTRODUCTION

Parkinson's disease (PD) is characterized by a progressive degeneration of dopaminergic (DA) neurons located in the substantia nigra pars compacta (SNc). This neuronal loss disrupts the function of the basal ganglia, a highly organized network crucial for goal-directed behavior and action selection (Mink, 1996; Redgrave et al., 1999; 2010). A classical theory regarding PD pathophysiology states that GABAergic neurons from the substantia nigra pars reticulata (SNr), a main output structure of the basal ganglia (Albin et al., 1989), become hyperactive following the loss of dopamine (Bergman et al., 1994; Hassani et al., 1996). This hyperactivity suggests that there is an intensified inhibitory influence of the SNr on its targets. Notably, the main structures receiving direct projections from the SNr are the thalamus such as the ventromedial thalamic nucleus (Carpenter, 1976; Clavier et al., 1976) and numerous structures in the brainstem, including the pedunculopontine tegmental nucleus, the superior colliculus (SC), the parabrachial nucleus (PBN) and the periaqueductal gray (PAG) (Hopkins et al., 1976; Schneider, 1986; Deniau and Chevalier, 1992; Spann and Grofova, 1991). While the thalamus and pedunculopontine tegmental nucleus have received considerable attention in PD research (Villalba et al., 2014; Blesa et al., 2016; Pahapill and Lozano, 2000, Tubert et al., 2019), the functional status of the SC, PBN, and PAG in PD remains relatively unexplored despite their close connectivity with the basal ganglia and the suggested pathological link between the SNr and these structures. We have previously demonstrated that the SC exhibits abnormal hypersensitivity to visual stimuli in PD rat models and *de novo* PD patients (Rolland et al., 2013; Moro et al., 2020). Additionally, we found diminished nociceptive responses in the PBN following a total DA lesion in the SNc (Pautrat et al., 2023). Our

previous work also provided indirect electrophysiological evidence suggesting that increased inhibitory input from the SNr in PD induces neuroplasticity changes in the SC and PBN (Rolland et al., 2013; Pautrat et al., 2023). On the basis of this evidence, we further investigated the anatomical, cellular, and molecular basis for neuroplasticity in the PBN. Our findings revealed an increase in density of dendritic spines, suggest their turnover is increased, and show decreased post-synaptic densities following partial or total DA lesions in the SNc. Furthermore, we found a significant increase in $GABA_A$ receptor expression in the PBN following a total DA lesion, but not a partial DA lesion (Pautrat et al., 2023).

Compensatory mechanisms in PD have been suggested to delay the clinical onset of the disease but also to play a role in the development of motor and non-motor symptoms (Blesa et al., 2017). Molecular and cellular compensatory mechanisms have mainly been studied within the basal ganglia (Bezard and Gross, 1998; Arkadir et al., 2014; Blesa et al., 2017) but our findings suggest that important changes can also take place at the level of their targets. These changes are likely to play a significant role in the pathological changes underlying PD as the disorder progresses. Having previously reported compensatory neuroadaptations in the PBN (Pautrat et al., 2023), our main objective in this study was to evaluate the cellular (using Golgi-Cox for spine density and morphology) and molecular (via Western blot for $GABA_A$ receptor expression) bases for neuroadaptive plasticity in both the SC and PAG in hemiparkinsonian rats with either a partial or total DA denervation in the SNc (Pautrat et al., 2023). Our hypothesis was that the SC and the PAG would show similar cellular and molecular changes to those described in the PBN since these structures also receive a direct projection from the SNr. The nigrotectal pathway heavily projects to the lateral part of the SC, and to a lesser extent to the medial

regions of this structure (Harting et al., 1988), and hence we performed a separate analysis on the medial and the lateral SC.

## 2 | METHODS

### 2.1 | Animals

Male Long Evans rats were used for these experiments. They were kept in standard environmental conditions (12 h light/dark cycle) at a constant temperature 22 °C, with food and water provided ad libitum. The experiments were carried out in accordance with the policy of Lyon 1 University, the Grenoble Institut des Neurosciences (GIN) and French legislation. Experiments were conducted in compliance with the European Community Council Directive of November 24, 1986 (86/609/EEC). The research was authorized by the Direction Department of Veterinary Services of Isère - Ministry of Agriculture and Fisheries, France (Coizet, Véronique, PhD, permit number 381003). Every effort was made to minimize the number of animals used and their suffering during the experimental procedures. All procedures were reviewed and validated by the “Comité éthique du GIN n°004” agreed by the research ministry.

### 2.2 | 6-OHDA lesions

Male Long Evans rats (n=63) were anaesthetized with isoflurane gas and placed in a stereotaxic frame. Their heads were shaved, cleaned and disinfected with Vétédine®. Animals were given a subcutaneous injection of a local anesthetic (Lidocaine) before a midline incision was performed and the scalp retracted to allow access to the skull. A burr-hole was then drilled above the SNc on the right hand side of midline, and the toxin 6-

hydroxydopamine (6-OHDA) (Sigma-Aldrich, USA, 2.6 $mg.mL^{-1}$) was injected with a 30G cannula connected with polyethylene tubing to a 10µL Hamilton syringe, driven by an infusion pump at 0.5µL/min. At the end of the injection, the cannula was kept in place for 5 min to allow the toxin to diffuse.

Three animal groups were prepared:

i) Partial DA lesion animals (Partial DA lesion, n = 14) received 1.0 µL of 6-OHDA at the following coordinates: Antero-posterior (AP): +3.0 mm; Medio-lateral (ML): +2.4 mm and Dorso-ventral (DV): +2.4 mm from interaural zero.

ii) Total DA lesion animals (Total DA lesion, n = 25) received 3.0 µL of 6-OHDA at the following coordinates: AP: +3.0 mm; ML: +2.1 mm and DV: +2.5 mm from interaural zero.

iii) Control animals received vehicle (sterile 0.9% NaCl) without the toxin (Sham, n = 24) at the following coordinates: AP: +3.0 mm; ML: +2.4 mm and DV: +2.4 mm from interaural zero.

These coordinates were calculated according to the rat brain atlas of Paxinos and Watson (2007). The DA degeneration occurs during the first two weeks' post-injection of the toxin, before reaching a baseline during the third week.

### 2.3 | Golgi staining

Three weeks after the 6-OHDA lesion, rats (n=3 in each experimental group) were euthanized with an overdose of pentobarbital (150 mg/kg, i.p.) and perfused with 250 mL of 0.9% saline followed by 250 mL of 4% formaldehyde. The brains were collected and placed in 4% formaldehyde overnight for post-fixation, and then placed in Golgi-Cox solution (1% potassium dichromate, 1% potassium chromate, 1% mercuric chloride) for

two days. The solution was then replaced by a fresh one and the brains were immersed for 12 more days. The incubation (total of 14 days) was done in the dark at room temperature. Afterwards, the brains were washed in 1% potassium dichromate for 24 h, placed in 20% sucrose for 24 h for cryo-protection and then snap-frozen in -60°C isopentane. Two series of sagittal brain sections were cut. The first one consisted of 30µm thick slices centered on the SNc (AP: -5.2/-5.8 mm behind bregma) and was collected in anti-freeze solution and stored at -20°C for anti-tyrosine hydroxylase (TH) immunohistochemistry. The second one consisted in 80 µm thick slices centered on the SC and PAG collected directly onto gelatin-coated slides. This thickness and sagittal orientation allowed optimal preservation of the tissue and observation of spines on the secondary and tertiary dendritic segments. Indeed, unlike the PBN (Pautrat et al., 2023), it was not possible to identify a dendrite with sufficient length and observe sufficient dendritic spines when using coronal sections. Microscope slides were then developed with Kodak rapid fix diluted at 1:6 in distilled water, dehydrated in alcohols and coverslipped in DPX. Slides were allowed to dry at room temperature for 72 h, after which they were cleaned and scanned.

### 2.4 | Golgi RECONSTRUCT

Slides stained with the Golgi-Cox technique were scanned using Zeiss Axio Scan.Z1 (Zeiss, Germany) at 40x magnification. 10 Z-stacks with a 2.0µm step were taken, centered on either the entire SC or PAG region. Images were imported into RECONSTRUCT software that utilizes the distinct geometric characteristics of spines for their categorization (Fiala, 2005; Risher et al., 2014). Dendritic sections of neurons clearly

located in the deep lateral and medial SC and in the lateral/ventrolateral PAG were analyzed. With the RECONSTRUCT software, the experimenter identified each dendritic segment to analyze by drawing a line along the dendrite (which in every case was clearly connected to a cell body, Figure 1A) as well as along the shafts of the associated dendritic spines and across the width of the spine heads. The software then extracted measurements based on the selected dendrites and spines. Parameters such as spine length, width and number were then measured. The software classifies spine morphology automatically based on these measurements, providing information such as dendrite length, width, total spine count, percentage of mushroom / stubby / filopodial / branched / long thin / thin spines, and spine density. This approach utilizes the distinct geometric characteristics of spines as the basis for their categorization (see Figure 1B, Risher et al. 2014):

- Filopodial: Length > 2 µm;
- Long thin: Length > 1 µm and ≤ 2 µm;
- Thin: Length ≤ 1 µm;
- Stubby: Length/Width ration < 1;
- Mushroom: Width > 0.6 µm;
- Branched: 2 heads or more.

According to Risher et al. (2014), with this method, users can expect to spend considerably less time and conduct an unbiased classification of spines. Quantification achieved with this method can also be reliably compared to data obtained from other users, providing some much needed consistency to the analysis of spines.

We analyzed the dendritic spines density and spine morphology as follow:

- n ≥ 5 dendrites per animal (each from a different neuron)
- Total length of dendritic segments analyzed per animal: 600 µm
- 3 animals per experimental group
- Total dendritic length analyzed per group: ~1800 µm (~600 X 3)

The number of dendrites was used as the sample size for statistical analysis.

In addition to the current Golgi experiments conducted in the SC and PAG, we analyzed Golgi data from the PBN obtained in a previous study (Pautrat et al., 2023). The experimental groups, the number of rats per group (N = 3), and the methodology for Golgi staining were identical to those used in the present study.

### 2.5 | Western blot

This analysis included a total of 30 rats for the Lateral SC (Sham: n = 9; Partial DA group: n = 8; Total DA group: n = 13), 45 rats for the Medial SC (Sham: n = 17; Partial DA group: n = 11; Total DA group: n = 17) and 27 rats for the PAG (Sham: n = 7; Partial DA group: n = 9; Total DA group: n = 11). Three weeks after the 6-OHDA lesion, animals were deeply anesthetized using isoflurane before immediate decapitation and brain sampling. The brains were quickly frozen in isopentenyl (-60°C) and two series of coronal brain sections were cut in a cryostat. The first consisted of 30µm slices centered on the SNc (AP: -5,2/-5,8 mm behind Bregma) collected on slides for anti-TH immunohistochemistry. The second one consisted in 80µm thick slices centered on the entire anterior-posterior length of the SC and PAG. The lateral SC, medial SC and PAG were then isolated using a tissue punch and all samples were stored at –80° until Western blot processing. The samples

were then homogenized in a cold 10% sodium dodecyl sulfate (SDS) solution with a protease inhibitor cocktail tablet (Sigma-Aldrich, USA). The homogenized solution was centrifuged at 15,000 x g for 15 min at 4 °C and the clear supernatant was collected. Following a BCA protein assay, the samples were diluted and mixed with 4X SDS sample buffer (Laemmeli with beta mercaptoethanol, Bio-Rad Laboratories, USA), boiled at 95˚C for 10 min, cooled and then centrifuged at 10,000 x g for 2 min. Equal amounts of protein (20 µg) for each group were resolved using 10% SDS-PAGE. Proteins were then electrophoretically transferred to a PVDF membrane (GE Healthcare, Germany) for 1 h 15 min. The transferred proteins were then blocked with 3% bovine serum albumin (BSA) in TBS-T for 2 h at room temperature. The blot was then incubated overnight at 4°C with the following primary antibodies: rabbit anti-$GABA_AR$ α1 (1:2000, Sigma-Aldrich, Germany), and rabbit anti-GAPDH (1:2000, Sigma-Aldrich, USA). After incubation, the blots were washed with TBS-T three times for 10 min each. The blots were incubated with anti-rabbit horseradish peroxidase-conjugated secondary antibody (1:10,000, Cell Signaling, USA) for 2 h. After washing three times (each wash for 10 min), ECL Plus substrate (Thermofisher, USA) was applied to the blots for 5 min in the dark. The blots were revealed using the Chemidoc Imaging System (Bio-Rad Laboratories, USA) and the protein expression intensity was assessed by integrated optical density (IOD). To account for possible differences in total protein load, the results of the measurements were presented as a ratio of IOD of $GABA_A$ receptor protein to the IOD of the respective GAPDH using ImageJ software (Bio-Rad Laboratories, USA).

### 2.6 | Histology 6-OHDA lesions

The extent of the DA denervation induced by 6-OHDA injections in the SNc was determined in all animals from this experiment using TH immunohistochemistry on free-floating slices (Golgi-Cox material) or directly on slides (Western blot material). To reveal TH, the sections were washed and incubated in a blocking solution containing 0.1M phosphate buffer (PB) with 0.3% of Triton X-100 (TX), 2.5% BSA and 5% normal horse serum (NHS) for 2 h before being transferred overnight to a 0.1M PB-TX 0.3% with 1% BSA and 2% NHS containing the primary mouse monoclonal TH antibody, diluted 1:3000 (Chemicon, UK). The following day, sections were washed in 0.1M PB and incubated with the secondary antibody, biotinylated anti-mouse made in horse (in a dilution of 1:1000 in 0.1M PB-TX 0.3% with 2% NHS) for 2 h. Following further washes in 0.1M PB, the sections were exposed to the elite Vectastain ABC reagent (Vector Laboratories, USA) diluted 1:100 in PB-TX 0.3%, for 2 h. Again, following washes in 0.1M PB, immunoreactivity was revealed by exposure to nickel enhanced 3,3'-diaminobenzidine (DAB, Sigma-Aldrich, USA) for 2 min, which produced a black reaction product. Sections were then mounted onto gelatin-coated slides, dehydrated through alcohols and cleared in xylene before being cover slipped with DPX. TH immunolabeling of DA neurons in the SNc (– 6.00 to – 6.30 mm AP relative to bregma, one section / rat) was evaluated using a light microscope (Nikon Eclipse 80i, TRIBVN, France) coupled to the ICS Framework computerized image analysis system (TRIBVN, 2.9.2 version, France). For quantification, TH-labelled sections of the SNc were digitized using a Pike F-421C camera (Allied Vision Technologies, Germany). Optical densities (OD) were then measured in all animals from this experiment for the denervated hemisphere (right) and non-denervated hemisphere (left) of operated animals. OD of the lesioned hemisphere was then compared to the non-lesioned hemisphere in each animal.

In all animals from this experiment, we used a stereo investigator software (Stereo Investigator 2022.3.1, MFB Bioscience LLC, Williston, VT USA) to manually count TH cells in the SNc. The SNc was delineated with a 2 X objective (Olympus, BX53) at the level of – 6.00 to – 6.30 mm AP relative to bregma (one section / rat). Cell counting was performed using a 40X objective throughout the SNc, with a 100% sampling grid and a 60 x 60 µm counting frame.

### 2.7 | Statistics

All statistical tests were performed using GraphPad Prism v6.01 (Dotmatics, USA) software. The Shapiro-Wilk test was used to assess the normality of the different data distributions. The statistical reliability of differences between the three groups for all data was assessed using ANOVA analysis followed by Tukey post-hoc multiple comparison test or a Kruskal-Wallis analysis followed by Dunn's post-hoc multiple comparisons according to the normality of the distribution of the data. Significance threshold was set at $p < 0.05$.

## 3 | RESULTS

### 3.1 | Histological analysis of the dopaminergic lesion

To analyze the extent of the DA lesion induced by the injection of 6-OHDA into the SNc in the animals used in the Western blot and Golgi-Cox experiments, we used TH immunohistochemistry. Similar to our previous experiments (Rolland et al., 2013; Pautrat et al., 2023), in addition to Sham animals, two experimental groups were defined according to the extent of the DA degeneration: Partial and Total DA lesion groups. The

Sham group received an injection of sterile saline unilaterally in the SNc instead of the toxin (N = 24).

TH-labelling in the SNc on the lesioned side in the Partial DA lesion group was reduced to an average of 52.13 ± 5.44 % (mean ± standard error of the mean, SEM) of the unlesioned side, with the remaining DA neurons located in the medial part of the SNc (N = 14). In the Total DA lesion group, only 13.16 % ± 2.08 % (mean ± SEM) of TH-labeled neurons remained in the lesioned SNc (N = 25). The difference between these groups in terms of percentage of remaining TH-labelling was statistically significant ($F[2, 60] = 174,4$, $p < 0.001$).

The survival of the nigral DA neurons was further analyzed by stereological counting of TH cells in the SNc. The analysis revealed a main effect of the Lesion (Kruskal-Wallis, $K= 39.99$, $p < 0.0001$, followed by Dunn's multiple comparisons test; Number of TH cells, mean ± SEM: Sham = 422.80 ± 3.10; Partial DA lesion: 166.50 ± 22.80; Total DA lesion: 57.33 ± 6.48).

Both methods reveal significant differences between the three experimental groups when considering the extent of 6-OHDA lesions in the SNc. The lesions have been illustrated in Supplementary Figure 1.

### 3.2 | Golgi-Cox analysis of dendritic spine density and morphology

Dendritic spines are a well-recognized locus of change when studying adaptive neuroplasticity (Risher et al., 2014; Trachtenberg et al., 2002). We have previously shown that Partial and Total DA lesion groups exhibit an increased density of dendritic spines in the PBN compared to Sham, in particular an increase of filopodial and branched spines

types (Pautrat et al., 2023). Given that the SC and PAG share the same connectivity with the basal ganglia as the PBN (for review, see Coizet et al., 2024), a similar change at the level of the spines was expected. Following Golgi-Cox staining in the SC and PAG, and using RECONSTRUCT, an average of ~600 µm of dendrites were analyzed in each rat, according to the method developed by Risher and collaborators (2014). After counting and measuring the spines, the software categorized their morphology as filopodial, thin, long thin, stubby, mushroom or branched (Figure 1). Here, we first present an analysis of the type of dendritic spines found in sham animals in the lateral SC, medial SC and PAG as to our knowledge, this characterization had never been reported previously. As the analysis of the dendritic spine morphology in the PBN was not included in our previous work (Pautrat et al., 2023), we have also included it here for comparison. After an account of dendritic spine morphology in sham animals, next we analyzed the effect of DA lesions on the morphology of dendritic spines in the lateral SC, medial SC and PAG.

#### 3.2.1 | Morphology of dendritic spines in the sham group

##### 3.2.1.1 | Lateral superior colliculus

We found a significant difference in the spine type densities within the lateral SC of Sham rats (Kruskal-Wallis, $K = 175.2$, $p < 0.001$, followed by Dunn's multiple comparisons test, Mean ± SEM in Table 1). Overall, the dendritic spine morphology found in the lateral SC is largely of thin type (75 %) and to a lesser extent stubby (15 %) and long thin types (7,5 %). Only a small proportion (1 to 1.5 %) of mushroom, filopodial and branched types were found (Figure 2A).

#### 3.2.1.2 | Medial superior colliculus

Similar to the lateral SC, analysis of the spine density and morphology in the Sham group showed a significant difference in the density of the different spine types (Kruskal-Wallis, $K = 156.7$, $p < 0.001$, followed by Dunn's multiple comparisons test, Mean ± SEM in Table 1). Overall, the dendritic spine morphology found in the medial SC is largely of thin type (74 %) and to a lesser extent stubby (15 %) and long thin types (6 %). Only a small proportion (1 to 3%) of mushroom, filopodial and branched types were found (Figure 2B).

#### 3.2.1.3 | Periaqueductal gray

Analysis of the spine morphology of Sham animals also revealed a significant difference in the dendritic spine types (Kruskal-Wallis, $K= 136.5$, $p < 0.001$, followed by Dunn's multiple comparisons test, Mean ± SEM in Table 1). The dendritic spine morphology found in the PAG is largely of thin type (74 %) and to a lesser extent long thin (14 %) and stubby types (9 %). Again, only a small proportion (0.4 to 2 %) of mushroom, filopodial and branched types were found (Figure 2C).

#### 3.2.1.4 | Parabrachial nucleus

Similarly to the SC and the PAG, analysis of the spine morphology of Sham animals also revealed a significant difference in the dendritic spine types (Kruskal-Wallis, $K= 60.91$, $p < 0.001$, followed by Dunn's multiple comparisons test, Number of cells: Mean ± SEM). However, the dendritic spine morphology found in the PBN is differently distributed compared to the SC and the PAG with a majority of mushroom (36 %) thin (23 %) and

stubby (19 %) types. Again, a smaller proportion (5 to 9 %) of long thin, filopodial and branched types were found (Figure 2D).

### 3.2.2 | Effect of dopaminergic lesions on dendritic spines

#### 3.2.2.1 | Lateral superior colliculus

The statistical analysis comparing Sham and DA lesioned rats revealed a significant increase in the spine density in the Total DA lesion group compared to both the Sham and Partial DA lesion groups (Kruskal-Wallis, $K = 44.93$, followed by Dunn's multiple comparisons test, $p < 0.001$). Further analysis of the spine morphology showed a significant increase of the thin spine type in the Total DA lesion group compared to both the Sham and Partial DA lesion groups (ANOVA, $F[2, 113] = 13.82$, followed by Tukey's multiple comparisons test, $p < 0.001$). The differences between the Sham and the Partial DA lesion groups were not statistically significant.

This analysis also revealed a significant change in the density of the stubby spine type (Kruskal-Wallis, $K = 36.41$, followed by Dunn's multiple comparisons test, $p < 0.001$). The extent of the DA lesion produced substantially different outcomes, with a significant decrease of this spine type in the Partial DA group (Partial DA lesion group vs Sham, $p < 0.05$; Partial DA lesion group vs Total DA lesion group, $p < 0.001$) and an increase in this spine type in the Total DA group (Total DA lesion group vs Sham, $p < 0.05$). A trend toward an increase of the mushroom spine type density was also found in both DA lesion groups (Kruskal-Wallis, $K = 4.767$, followed by Dunn's multiple comparisons test, $p = 0.09$). The other types of spines were not changed by the DA lesion (branched, filopodial, long thin). (Figure 3A and D, Mean ± SEM in Table 1).

#### 3.2.2.2 | Medial superior colliculus

Statistical analysis of the medial SC revealed a significant increase of the spine density in the Total DA lesion group when compared to both the Sham and Partial DA lesion groups (Kruskal-Wallis, K = 34.69, followed by Dunn's multiple comparisons test, $p < 0.001$). We found a significant increase in thin (Kruskal-Wallis, K = 17.99, followed by Dunn's multiple comparisons test, $p < 0.001$), stubby (Kruskal-Wallis, K = 41.28, followed by Dunn's multiple comparisons test, $p < 0.001$) and mushroom type spine density (Kruskal-Wallis, K = 7.97, followed by Dunn's multiple comparisons test, $p < 0.05$) in the Total DA lesion group compared to both the Sham and Partial DA lesion groups. The differences between the Sham and Partial DA lesion groups were not statistically significant. The other types of spine morphology were not altered by the DA lesion (Figure 3B and E, Mean ± SEM in Table 1).

#### 3.2.2.3 | Periaqueductal gray

Similar to the lateral SC, statistical analysis showed a significant increase in spine density in the PAG in the Total DA lesion group only (Kruskal-Wallis, K = 40.38, followed by Dunn's multiple comparisons test, $p < 0.001$). Analysis of the spine morphology revealed a significant increase of the thin (Kruskal-Wallis, K = 22.05, followed by Dunn's multiple comparisons test, $p < 0.001$), and stubby (Kruskal-Wallis, K = 52.68, followed by Dunn's multiple comparisons test, $p < 0.001$) spine types in the Total DA lesion group compared to both the Sham and the Partial DA lesion groups. The differences between the Sham and Partial DA lesion groups were not statistically significant. A trend toward a significant

increase of the mushroom spine type is also found (Kruskal-Wallis, K = 5.174, followed by Dunn's multiple comparisons test, p = 0.07) (Figure 3C and F, Mean ± SEM in Table 1).

### 3.3 | Western blot analysis of $GABA_A$ receptor expression.

The second parameter of adaptive neuroplasticity that we investigated was the potential change in GABA receptor expression as a consequence of increased activity in SNr projections to the SC and the PAG following DA denervation. The $GABA_A$ receptor is the most common receptor at inhibitory synapses such as those present between the SNr and the SC/PAG (Oertel and Mugnaini, 1984) and we have previously found total DA lesions to lead to increased levels of $GABA_A$ receptors in the PBN (Pautrat et al., 2023). Western blot analysis was therefore used to detect and compare the possible change in $GABA_A$ receptors expression in the SC and the PAG between the three experimental groups.

#### 3.3.1 | Lateral superior colliculus

In this experiment, we compared the Sham (n = 9), Partial (n = 9) and Total (n = 11) DA lesion groups in terms of $GABA_A$ receptor expression in the lateral SC. A significant increase of $GABA_A$ receptor expression was found in the Total DA lesion group compared to the Sham and Partial DA lesion groups (ANOVA, F [2, 23] = 3,843, $p < 0.05$) (Figure 4A, Mean ± SEM in Table 1).

#### 3.3.2 | Medial superior colliculus

We also compared the Sham (n = 15), Partial (n = 9) and Total (n = 15) DA lesion groups in relation to the medial SC. Unlike the lateral SC, analysis of the $GABA_A$ receptor

expression in the medial part of the SC did not show a statistical difference between the experimental groups (ANOVA, F [2, 36] = 0.022, p = 0.97) (Figure 4B, Mean ± SEM in Table 1).

### 3.3.3 | Periaqueductal gray

Finally, we compared Sham (n = 7), Partial (n = 9) and Total (n = 9) DA lesion groups in relation to the PAG. Similar to the medial SC, analysis of the $GABA_A$ receptor expression in the PAG did not show a statistical difference between the experimental groups (ANOVA, F [2, 22] = 1,501, p = 0.2449) (Figure 4C, Mean ± SEM in Table 1).

## 4 | DISCUSSION

We previously described the presence of neuroplasticity at the level of the density of dendritic spines and expression of $GABA_A$ receptors within the PBN in two rat models of PD with partial or total DA degeneration in the SNc (Pautrat et al., 2023) With the SC and the PAG sharing the same connectivity with the basal ganglia as the PBN and the hyperactivity of SNr GABAergic projections to the SC and PAG in the context of PD, we expected that a similar change would be found within these structures in the same rat models of PD - this issue has never been studied previously. However, unlike the PBN, the overall spine density was largely unaffected in the Partial DA lesion group in both the SC and the PAG. However, the Total DA lesion group showed an increase spine density in the medial and lateral SC, and in the PAG. An increase in $GABA_A$ receptor expression was also found in the lateral SC in this group.

### 4.1 | Functional implications of spine morphology

Most of the literature on dendritic spines concerns the cortex or the hippocampus, within which spine genesis, function and dynamics remain a topic of discussion (Pchitskaya and Bezprozvanny, 2020; Rasia-Filho et al., 2023). Spines on neurons in subcortical structures have received comparatively little attention and it is instructive to consider the functional implications of our findings. It has been suggested that the function of dendritic spines is not simply linked to the size of the dendritic surface available for synaptic contacts. Using a computational approach, Segev and Rall (1988; 1998) proposed that the width of the spine neck influences its electrical resistance, thereby affecting the extent to which synaptic inputs on the spine influence the somatic membrane potential. Thin spine necks will increase the spine stem resistance, leading to large local excitatory and inhibitory postsynaptic potentials (EPSPs and IPSPs) at the level of the spine head. These may have comparatively little effect on the somatic membrane potential and hence the likelihood of spike activity. However, we also found that stubby spine densities are strongly increased in these structures, especially in the PAG. Stubby spines have a large head, similarly to mushroom spines, and no obvious constriction between the head and the attachment to the shaft. A wider spine stem might be expected to reduce local EPSPs and IPSPs in the spine head, although due to decreased resistance, those local potentials are likely to influence spike activity in a way that the corresponding potentials in thin spines would not.

### 4.2 | Impact of dendritic spine morphology on plasticity

At the level of the dendritic spines, it is interesting to note several discrepancies between these midbrain structures, the SC / PAG, and the PBN, located at the junction between the pons and the midbrain. In both the PAG and the SC (whether the medial or the lateral regions), the majority of spines have a thin type morphology, and to a lesser extent, stubby and long thin morphology. Unlike the SC/PAG, the majority of spines in the PBN have a mushroom type morphology, followed by thin and stubby types. Following a DA lesion in the SNc, these types of spines in the PBN remained stable but branched and filopodial types increased in density (Pautrat et al., 2023), while in the SC and PAG, thin and stubby spines densities increased. The morphology of the spines may thus represent an important factor underlying plasticity in a pathological context.

### 4.3 | Impact of increased $GABA_A$ receptor expression

We and others have previously shown that DA lesions lead to an elevation in the firing rate of neurons in the SNr (Breit et al., 2006; Pautrat et al., 2023; Diaz et al., 2003; Waszczak and Walters, 1984), which will increase inhibitory tone in structures receiving an input from the SNr. Postsynaptic plasticity following repeated presynaptic activation has previously been associated not only with an increase excitatory synapses but also in GABAergic synapses on spines (Mele et al., 2016; Knott et al., 2002), which the increase in $GABA_A$ receptor expression that we report suggests may be happening in the lateral SC. Furthermore, it has also been shown at the level of the hippocampus that long term potentiation (LTP), an electrophysiological model of neuronal plasticity, is associated with enlargement of the spine head and shortening of the spine neck or the induction of short, stubby spines and thus changes in synaptic strength and EPSPs (see Rasia-Filho et al.,

2023 for review). With the significant increase of stubby spines following a DA lesion in the SC and PAG, the potential presence of LTP implies that these changes at the level of the spines are likely to be become long lasting in the context of PD. Evidence of the presence of LTP is further supported, at least in the lateral SC, by our finding of increased $GABA_A$ receptor levels in this part of the SC. Indeed, $GABA_A$ receptors mediate fast synaptic inhibition by controlling rapid chloride ion flow, which is critical for the timing and modulation of synaptic strength. This rapid response is essential for LTP and LTD at inhibitory synapses (Chiu et al., 2019). It has been shown at the level of the hippocampus that increased numbers of synaptic $GABA_A$ receptors underlies potentiation of GABAergic neurotransmission in this structure (Nusser et al., 1998). This raises the possibility that post-synaptic insertion of new $GABA_A$ receptors in the lateral SC may increase the efficacy of inhibitory synapses underlying long lasting and marked alteration of synaptic transmission. The limitation of $GABA_A$ receptor changes to the medial SC may come down to the fact that the nigrotectal pathway heavily projects to the lateral part of the SC, and to a lesser extent to the medial regions of this structure (Harting et al., 1988). Note that the effect of increased $GABA_A$ receptors in the lateral SC may not be restricted to neurons alone. Astrocytes express ionotropic $GABA_A$ receptors and are thus “GABA-receptive cells”, at least in the thalamus, hippocampus and cerebellum (Jiménez-González et al., 2011; Lee et al., 2010; Wang et al., 2024). It has been proposed that $GABA_A$ receptors expressed in astrocytes could also play a role in maintaining inhibitory tone and supporting neuroplasticity, such as the increase in stubby and thin spine types we observed. Furthermore, it has been shown that microglia play a variety of roles in synaptic plasticity. One such role includes synapse elimination via phagocytosis (Andoh and Koyama, 2021).

### 4.4 | Neuroplasticity and substantia nigra pars reticulata connectivity

We found a discrepancy between the SC/PAG and the PBN in terms of the effect of the extent of the DA lesion on dendritic spine neuroplasticity. Within the PBN, a partial DA lesion in the SNc was found to be enough to induce an increase of spine density similar to that found following a total DA lesion (Pautrat et al., 2023). However, that was not the case for the SC (whether the medial or the lateral part) or the PAG, where a total DA lesion was required to change spine density. This result is surprising at the level of the SC since both partial and total DA lesions produce a visual sensory rebound in the SC measured electrophysiologically (Rolland et al., 2013), similarly to the PBN with noxious stimuli (Pautrat et al., 2023). This could suggest that other types of neuroplasticity, not studied in our work, may be found within the SC and PAG of animals with partial DA lesions which should be explored further.

The possibility exists that the differences we have found between the internal micro-organization of each structure studied may also come down to the type and strength of the SNr projections onto the SC/PAG and PBN. Cumulative evidence from the literature refutes the classical assumption of the neurochemically and neuroanatomically homogeneous nature of the SNr. An early study described the SNr as containing both GAD positive and GAD negative cells (Oertel and Mugnaini, 1984). Kha and colleagues (2001) then highlighted the diversity of neurochemicals within the SNr, with neurons reactive to antibodies against GABA, glutamate, choline acetyltransferase, and the vesicular acetylcholine transporter. Note that glutamate is the metabolic precursor of GABA. Therefore, immunoreactivity for glutamate should not be taken as an indication of the presence of glutamatergic neurons among a large population of GABAergic neurons.

This is coherent with the finding that the SNr provides an output to the thalamic nucleus reticularis with an excitatory component in parallel with the classical inhibitory output to the ventroposterolateral nucleus and both excitatory and inhibitory output to the posterior nucleus of the thalamus (Antal et al., 2014). A similar variability of SNr influence may also be found for the brainstem structures. Anatomically, McElvain and colleagues (2021) recently found that the SNr contained distinct pools of neuronal projections differentially targeting structures from the brainstem, each pool having specific electrophysiological properties. A subset of SNr neurons targets the lateral SC which differs from the subset targeting the medial SC, the PAG and the PBN (McElvain et al., 2021). In addition to these physiological data, it has been shown that a DA lesion differentially impacts SNr neurons according to their nature (Delgado-Zabalza et al., 2023). Parvalbumin positive neuronal firing rate is altered, but not parvalbumin negative neurons. Altogether, these data from the literature highlight that the link between the SNr and its targets is more complex than originally thought, with a larger diversity of projections in term of cell type, physiology and strength.

## 5 | LIMITATIONS

We feel it is important to briefly draw attention to a couple of limitations in the present work. Our analysis indicates a strong plasticity at the level of the dendritic spines, with an increase of thin and stubby spines types within the SC and PAG in animals with a total DA lesion and increased $GABA_A$ receptor expression in this group in the lateral SC. However, our analysis was performed three weeks after the lesion and we cannot exclude the possibility of additional changes to these parameters may have occurred after a longer

delay. Furthermore, changes observed might also represent an early stage plasticity that may not persist in time.

The structural changes found at the level of the dendritic spines and the changes in receptor expression suggest that synapses themselves may be altered, although this has not been assessed in the present work. Additional experiments using electron microscopy should now be performed to fully evaluate the shape of the post-synaptic density following DA lesions, which we have shown to be reduced in the PBN (Pautrat et al., 2023) and may further impact synaptic transmission. Electrophysiological experiments are also crucial to perform to assess changes in synaptic strength. We also cannot exclude the possibility of additional neuroplasticity impacting the glutamatergic system with glutamatergic synapses located on the head of the spines. Overall, neuroplasticity mechanisms within the brainstem, a major direct target of the basal ganglia, to our knowledge have hardly been studied before. Our previous work (Pautrat et al., 2023), in addition to the present experiments, provide the first evidence of such a mechanism in the PBN, SC and PAG in the context of PD. Finer analysis is now needed to compare anatomical and structural changes in neurons directly connected with the SNr with those which are not connected to fully confirm the impact of the SNr in the neuroplasticity observed in our regions of interests. We also have based our analysis on the anatomical and molecular plasticity occurring within the SC and the PAG but not the functional consequences of that plasticity in terms of the development of non-motor symptoms in PD such as attentional deficits or pain symptoms, in which the SC and the PAG could be involved, respectively (Tovote et al., 2016; Basso et al., 2021).

Finally, as reviewed by Rasia-Filho and colleagues (2023), human dendritic spines are similar in shape when compared to other animals, but dendritic spines have reached

higher levels of complexity in humans. Human spines show a diverse shape spectrum compared to other species, thus care should be taken in extrapolating our results in a clinical context and specific analysis of human tissue is crucial to confirm such mechanisms on PD.

## 6 | CONCLUSION

In conclusion, the connectivity between the SNr and other brainstem nuclei is poorly characterized and understood. Earlier, we have shown that structures such as the SC and the PBN exhibit altered sensory processing following the degeneration of DA neurons (Rolland et al., 2013; Pautrat et al., 2023) and in the present work that the SC and PAG, similarly to the PBN (Pautrat et al., 2023) showed an internal anatomical reorganization. Further work is required to explore in more details the link between the basal ganglia and the brainstem, especially at the level of the SNr output, to fully evaluate the functional impact PD could generate in these structures.

## AUTHOR CONTRIBUTIONS

Research project: (A) Conception: V.C and R.A.T. (B) Organization: V.C. and R.A.T (C) Execution: R.A.T. and R.S. (D) Statistical analysis: V.C, R.A.T and A.P.

Manuscript preparation: (A) Writing of the first draft: R.A.T. (B) Review and critique: V.C., P.G.O. (C) Writing and editing of final version: V.C.

## ACKNOWLEDGMENT

We thank the personnel from the animal facility for their technical contributions. This work was supported by the Photonic Imaging Center of Grenoble Institut des Neurosciences (Univ Grenoble Alpes—Inserm U1216) which is part of the ISdV core facility and certified by the IBiSA label.

## CONFLICT OF INTEREST STATMENT

The authors declare no competing interests.

## FUNDING SOURCES FOR STUDY

The work was funded by Inserm, and the “Network of Centers of Excellence in Neurodegeneration (CoEN)”. This work was supported by the École Doctorale Chimie et sciences du vivant, Université Grenoble Alpes.

## DATA AVAILABILITY STATMENT

The data that support the findings of this study are available from the corresponding author upon request.

## REFERENCES


Albin, R.L., Young, A.B. & Penney, J.B. (1989). The functional anatomy of basal ganglia disorder. *Trends in Neurosciences,* ***12(10)***, 366-375. https://doi.org/10.1016/0166-2236(89)90074-x

Andoh, M., and Koyoma, R. (2021). Microglia regulate synaptic development and plasticity. Developmental Neurobiology, **81(5)**, 568-590.

Antal, M., Beneduce, B.M. & Regehr, W.G. (2014). The substantia nigra conveys target-dependent excitatory and inhibitory outputs from the basal ganglia to the thalamus. *Journal of Neuroscience,* ***34(23)***, 8032-42. https://doi.org/10.1523/JNEUROSCI.0236-14.2014

Arkadir, D., Bergman, H. & Fahn, S. (2014). Redundant dopaminergic activity may enable compensatory axonal sprouting in Parkinson disease. *Neurology,* ***82(12)***, 1093-1098. https://doi.org/10.1212/WNL.0000000000000243

Basso, M.A., Bickford, M.E. & Cang, J. (2021). Unraveling circuits of visual perception and cognition through the superior colliculus. *Neuron,* ***109(6)***, 918-937. https://doi.org/10.1016/j.neuron.2021.01.013

Bergman, H., Wichmann, T., Karmon, B. & DeLong, M. (1994). The primate subthalamic nucleus. II. Neuronal activity in the MPTP model of parkinsonism. *Journal of Neurophysiology,* ***72(2)***, 507–520. https://doi.org/10.1152/jn.1994.72.2.507

Bezard, E. & Gross, C.E. (1998). Compensatory mechanisms in experimental and human parkinsonism: towards a dynamic approach. *Progress in Neurobiolgy,* ***55(2)***, 93-116. https://doi.org/10.1016/s0301-0082(98)00006-9

Blesa, J., Trigo-Damas, I. & Obeso, J.A. (2016). Parkinson's disease and thalamus: facts and fancy. *Lancet Neurology,* ***15(7)***, e2. https://doi.org/10.1016/S1474-4422(16)30048-5

Blesa, J., Trigo-Damas, I., Dileone, M., Lopez-Gonzalez Del Rey, N., Hernandez, L.F. & Obeso, J.A. (2017). Compensatory mechanisms in Parkinson's disease: Circuits adaptations and role in disease modification. *Experimental Neurology,* ***298(Pt B)***, 148-161. https://doi.org/10.1016/j.expneurol.2017.10.002.

Breit, S., Lessmann, L., Unterbrink, D., Popa, R.C., Gasser, T. & Schulz J.B. (2006) Lesion of the pedunculopontine nucleus reverses hyperactivity of the subthalamic nucleus and substantia nigra pars reticulata in 6-hydroxydopamine rat model. *European Journal of Neuroscience,* ***24***, 2275-2282. 10.1111/j. https://doi.org/1460-9568.2006.05106.x

Carpenter, M.B. (1976). Anatomy of the basal ganglia and related nuclei: a review. *Advances in Neurology,* ***14***, 7-48.

Chiu, C.Q., Barberis, A. & Higley, M.J. (2019) Preserving the balance: diverse forms of long-term GABAergic synaptic plasticity. Nature reviews Neuroscience, 20(5), 272-281. https://doi.org/10.1038/s41583-019-0141-5

Clavier, R.M., Atmadja, S. & Fibiger, H.C. (1976). Nigrothalamic projections in the rat as demonstrated by orthograde and retrograde tracing techniques. *Brain Research Bulletin,* ***1(4)***, 379-84. https://doi.org/10.1016/0361-9230(76)90031-9

Coizet, V., Al Tannir, R., Pautrat, A. & Overton PG. (2024). Separation of Channels Subserving Approach and Avoidance/Escape at the Level of the Basal Ganglia and Related Brainstem Structures. *Current Neuropharmacology,* ***22(9)***, 1473-1490. https://doi.org/10.2174/1570159X21666230818154903

Delgado-Zabalza, L., Mallet, N.P., Glangetas, C., Dabée, G., Garret, M., Miguelez, C. & Baufreton, J. (2023). Targeting parvalbumin-expressing neurons in the substantia nigra pars reticulata restores motor function in parkinsonian mice. *Cell Reports,* ***42(10)***, 113287. https://doi.org/10.1016/j.celrep.2023.113287

Deniau, J.M. & Chevalier, G. (1992). The lamellar organization of the rat substantia nigra pars reticulata: distribution of projection neurons. *Neuroscience,* ***46(2)***, 361–377. https://doi.org/10.1016/0306-4522(92)90058-a

Diaz, M.R., Barroso-Chinea, P., Acevedo, A., & Gonzalez-Hernandez, T. (2003) Effects of dopaminergic cell degeneration on electrophysiological characteristics and GAD65/GAD67 expression in the subtantia nigra: different action on GABA cell subpopulations. *Movement disorders,* ***18***, 254-266. https://doi.org/10.1002/mds.10345.

Fiala, J.C. (2005). Reconstruct: a free editor for serial section microscopy. *Journal of Microscopy,* ***218***, 52–61. https://doi.org/10.1016/0165-0270(80)90021-7

Harting, J.K., Huerta, M.F., Hashikawa, T., Weber, J.T. & van Lieshout, D.P. (1988). Neuroanatomical studies of the nigrotectal projection in the cat. *Journal of Comparative Neurology,* ***278(4)***, 615-631. https://doi.org/10.1002/cne.902780412

Hassani, O., Mouroux, M. & Féger, J. (1996). Increased subthalamic neuronal activity after nigral dopaminergic lesion independent of disinhibition via the globus pallidus. *Neuroscience,* ***72(1)***, 105–115. https://doi.org/10.1016/0306-4522(95)00535-8

Hopkins, D.A. & Niessen, L.W. (1976). Substantia nigra projections to the reticular formation, superior colliculus and central gray in the rat, cat and monkey. *Neuroscience Letters,* ***2(5)***, 253-259. https://doi.org/10.1016/0304-3940(76)90156-7

Jiménez-González, C., Pirttimaki, T., Cope, D.W. & Parri, H.R. (2011) Non-neuronal, slow GABA signalling in the ventrobasal thalamus targets δ-subunit-containing $GABA_A$ receptors. *European Journal of Neuroscience*, ***33***, 1482-2011. https://doi.org/10.1111/j.1460-9568.2011.07645.x

Kha, H.T., Finkelstein, D.I., Tomas, D., Drago, D., Pow, D.V. & Horne, M.K. (2001). Projections from the substantia nigra pars reticulata to the motor thalamus of the rat: Single axon reconstructions and immunohistochemical study. *Journal of Comparative Neurology, **440(1)***, 20–30. https://doi.org/10.1002/cne.1367

Knott, G.W., Quairiaux, C., Genoud, C. & Welker, E. (2002). Formation of dendritic spines with GABAergic synapses induced by whisker stimulation in adult mice. *Neuron, **34(2)***, 265-273. https://doi.org/10.1016/s0896-6273(02)00663-3.

Lee, S., Yoon, B-E., Berglund, K., Oh S-J., Park, H., Shin, H-S., Augustine, G.J. & Lee, C.J. (2010) Channel-mediated tonic GABA release from glia. *Science, **330***, 790-796. https://doi.org/10.1126/science.1184334

McElvain, L.E., Chen, Y., Moore, J.D., Brigidi, G.F., Bloodgood, B.L., Lim, B.K., Costa, R.M. & Kleinfeld, D. (2021). Specific populations of basal ganglia output neurons target distinct brain stem areas while collateralizing throughout the diencephalon. *Neuron, **109(10)***, 1721-1738.e4. https://doi.org/10.1016/j.neuron.2021.03.017

Mele, M., Leal, G. & Duarte, C. (2016). Role of $GABA_A$ R trafficking in the plasticity of inhibitory synapses. *Journal of Neurochemistry, **139(6)***, 997–1018. https://doi.org/10.1111/jnc.13742

Mink, J.W. (1996). The basal Ganglia: Focused selection and inhibition of competing motor programs. *Progress in Neurobiology, **50**,* 381-425. https://doi.org/10.1016/s0301-0082(96)00042-1

Moro, E., Bellot, E., Meoni, S., Pelissier, P., Hera, R., Dojat, M. & Coizet, V. (2020). Visual dysfunction of the superior colliculus in de novo parkinsonian patients. *Annals of Neurology,* ***87(4)***, 533-546. https://doi.org/10.1002/ana.25696

Nusser, Z., Hájos, N., Somogyi, P. & Mody I. (1998). Increased number of synaptic GABA(A) receptors underlies potentiation at hippocampal inhibitory synapses. *Nature,* ***395(6698)***, 172-177. https://doi.org/10.1038/25999

Oertel, W.H. & Mugnaini, E. (1984). Immunocytochemical studies of GABAergic neurons in rat basal ganglia and their relations to other neuronal systems. *Neuroscience Letters,* ***47(3)***, 233-238. https://doi.org/10.1016/0304-3940(84)90519-6

Pahapill, P.A. & Lozano, A.M. (2000). The pedunculopontine nucleus and Parkinson's disease. *Brain,* ***123(Pt 9)***, 1767-1783. https://doi.org/10.1093/brain/123.9.1767

Pautrat, A., Al Tannir, R., Pernet-Galley, K., Soutrenon, R., Vendramini, E., Sinniger, V., Overton, P.G., David, O. & Coizet, V. (2023). Altered parabrachial nucleus nociceptive processing may underlie central pain in Parkinson's disease. *NPJ Parkinson's Disease,* ***9(1)***, 78. https://doi.org/10.1038/s41531-023-00516-x

Paxinos, G. & Watson, C. (2007). The Rat Brain in Stereotaxic Coordinates. Academic Press, Sydney.

Pchitskaya, E. & Bezprozvanny, I. (2020). Dendritic Spines Shape Analysis-Classification or Clusterization? Perspective. *Frontiers in Synaptic Neuroscience,* ***12***, 31. https://doi.org/10.3389/fnsyn.2020.00031

Rasia-Filho, A.A., Calcagnotto, M.E., von Bohlen, U. & Halbach, O. (2023). Introduction: What Are Dendritic Spines? *Advances in Neurology,* ***34***, 1-68. https://doi.org/10.1007/978-3-031-36159-3_1

Redgrave, P., Prescott, T.J. & Gurney K. (1999). The basal ganglia: a vertebrate solution to the selection problem? *Neuroscience,* ***89(4),*** 1009-1023. https://doi.org/10.1016/s0306-4522(98)00319-4

Redgrave, P., Rodriguez, M., Smith, Y., Rodriguez-Oroz, M.C., Lehericy, S., Bergman, H., Agid, Y., DeLong, M.R. & Obeso, J.A. (2010). Goal-directed and habitual control in the basal ganglia: implications for Parkinson's disease. *Nature Reviews. Neuroscience,* ***11(11)***, 760-72. https://doi.org/10.1038/nrn2915

Risher, W., Ustunkaya, T., Alvarado, J. & Eroglu, C. (2014). Rapid golgi analysis method for efficient and unbiased classification of dendritic spines. *PLoS One,* ***9(9)***. https://doi.org/10.1371/journal.pone.0107591

Rolland, M., Carcenac, C., Overton, P., Savasta, M. & Coizet, V. (2013). Enhanced visual responses in the superior colliculus and subthalamic nucleus in an animal model of Parkinson's disease. *Neuroscience,* ***252***, 277-288. https://doi.org/10.1016/j.neuroscience.2013.07.047

Schneider, J. (1986). Interactions between the basal ganglia, the pontine parabrachial region, and the trigeminal system in cat. *Neuroscience,* ***19(2)***, 411–425. https://doi.org/10.1016/0306-4522(86)90271-x

Segev, I. & Rall, W. (1988). Computational study of an excitable dendritic spine. *Journal of Neurophysiology,* ***60(2)***, 499-523. https://doi.org/10.1152/jn.1988.60.2.499

Segev, I. & Rall, W. (1998). Excitable dendrites and spines: earlier theoretical insights elucidate recent direct observations. *Trends in Neuroscience,* ***21(11)***, 453-60. https://doi.org/10.1016/s0166-2236(98)01327-7

Spann, B.M. & Grofova, I. (1991). Nigropedunculopontine projection in the rat: an anterograde tracing study with phaseolus vulgaris-leucoagglutinin (PHA-L). *Journal of Comparative Neurology, **311(3)***, 375-388. https://doi.org/10.1002/cne.903110308

Tovote, P., Esposito, M.S., Botta, P., Chaudun, F., Fadok, J.P., Markovic, M., Wolff, S.B.E., Ramakrishnan, C., Fenno, L., Deisseroth, K., Herry, C., Arber, S. & Lüthi, A. (2016). Midbrain circuits for defensive behaviour, *Nature, **534(7606)***, 206-212. https://doi.org/10.1038/nature17996

Trachtenberg, J., Chen, B., Knott, G., Feng, G., Sanes, J., Welker, E. & Svoboda, K. (2002). Long-term in vivo imaging of experience-dependent synaptic plasticity in adult cortex. *Nature, **420(6917)***, 788–794. https://doi.org/10.1038/nature01273

Tubert, C., Galtieri, D. & Surmeier D.J. (2019). The pedunclopontine nucleus and Parkinson's disease. *Neurobiology of Disease, **128***, 3-8. https://doi.org/10.1016/j.nbd.2018.08.017

Villalba, R.M., Wichmann, T. & Smith, Y. (2014). Neuronal loss in the caudal intralaminar thalamic nuclei in a primate model of Parkinson's disease. *Brain Structure and Function, **219(1)***, 381-394. https://doi.org/10.1007/s00429-013-0507-9

Wang, D-S., Ju, L., Pinguelo, A.G., Kaneshwaran, K., Haffey, S.C., Lecker, I., Gohil, H., Wheeler, M.B., Kaustov, L., Ariza, A., Yu, M., Volchuk, A., Steinberg, B.E., Goldenberg, N.M. & Orser, A. (2024) Crosstalk between GABAA receptors in astrocytes and neurons triggered by general anesthetic drugs. *Translational research, **267***, 39-53. https://doi.org/10.1016/j.trsl.2023.11.007

Waszczak, B.L. and Walters, J.R. (1984) A physiological role for dopamine as modulator of GABA effects in substantia nigra: supersensitivity in 6-hydroxydopamine-lesioned rats. European Journal of Pharmacology, **105(3-4)**, 369-73.

Figure/Table legends

Figure 1: Golgi-Cox analysis: A. Photo micrographs illustrating the identification of dendritic spines clearly connected to a cell body (black arrow). Scale bar: 10 µm. B. Top panel: Photomicrographs of dendritic spines labelled with Golgi-Cox staining illustrating the different types of spines analyzed: Filopodial (red), long thin (orange), thin (yellow), stubby (green), mushroom (blue) and branched (purple). Bottom panel: Criteria used in the present study according to Richter et al. (2014) to classify the different spine types. Scale bar: 2 µm.

Figure 2: Histograms (mean ± SEM) (Top panels) and pie charts (Bottom panels) of the proportion of the dendritic spine morphologies measured in the Sham group in the lateral superior colliculus (A), the medial superior colliculus (B), the periaqueductal gray(C) and the parabrachial nucleus (D) in relation to the total spine density of these structures. The dendritic spine types were classified as mushroom (pink), filopodial (orange), branched (grey), long thin (yellow), stubby (dark blue) and thin (Green).
*: $p < 0.05$; **: $p < 0.01$; ***: $p < 0.001$.

Figure 3: Top panel: Histograms (mean ± SEM) of the total spine, thin spine, stubby spine and mushroom spine density measured in tissue labelled with Golgi-Cox staining in the Sham (blue), Partial (orange) and Total (red) DA lesion groups within the lateral superior colliculus (A), the medial superior colliculus (B) and the periaqueductal gray (C). Bottom panel: Photomicrograph montages (merge of different Z axes) of dendritic spines labelled with Golgi-Cox staining in the lateral superior colliculus (D), the medial superior colliculus

(E) and the periaqueductal gray (F) in the Sham (a, b, c, g, h, i, m, n, o) and Total DA lesion groups (d, e, f, j, k, l, p, q, s, t). Scale bar = 20 µm (Top and middle pictures), Scale bar = 5 µm (Bottom pictures).

*: $p < 0.05$; **: $p < 0.01$; ***: $p < 0.001$.

Figure 4: Histograms of $GABA_A$/GAPDH ratio (mean ± SEM) (Top panels) and individual examples of Western blot immuno-expression against GABA protein and GAPDH as a protein migration control (Bottom panels) measured using Western blot in the Sham (blue), Partial (orange) and Total (red) DA lesion groups within the lateral superior colliculus (A), the medial superior colliculus (B) and the periaqueductal gray (C).

* $p < 0.05$

Table 1: A. Mean ± SEM of the spine types in Sham rats (Golgi Cox, Spines/µm). B. Mean ± SEM of the spine density and spine types (Golgi Cox, Spines/µm) and $GABA_A$ receptor expression ($GABA_A$ / GAPDH ratio, Western blot) according to the structures and the experimental groups analyzed.

Supplementary figure 1: Histological analysis of the 6-OHDA lesions: A. Individual examples of sagittal section (Golgi-Cox experiment, top panel) and coronal sections (Western blot, bottom panel) labeled with TH immunohistochemistry in the Sham (left) Partial (middle) and Total (right) DA lesion groups. The red dotted lines delineate the SNc. The red arrows highlight areas with labelled DA cells and the white arrows highlight areas where TH labeling is missing, indicating a loss of DA cells. (scale bars=400 µm). (B) Histograms of the mean percentage (±SEM) of remaining TH labeling in SNc using optical

density analysis (left) and mean number (±SEM) of DA cells using stereology counting (right) in Sham (blue), Partial (orange) and Total (red) DA lesion groups. Measurements of TH immunoreactivity are compared to the intact side.

**: $p<0.01$; *** $p<0.001$

Figure 1

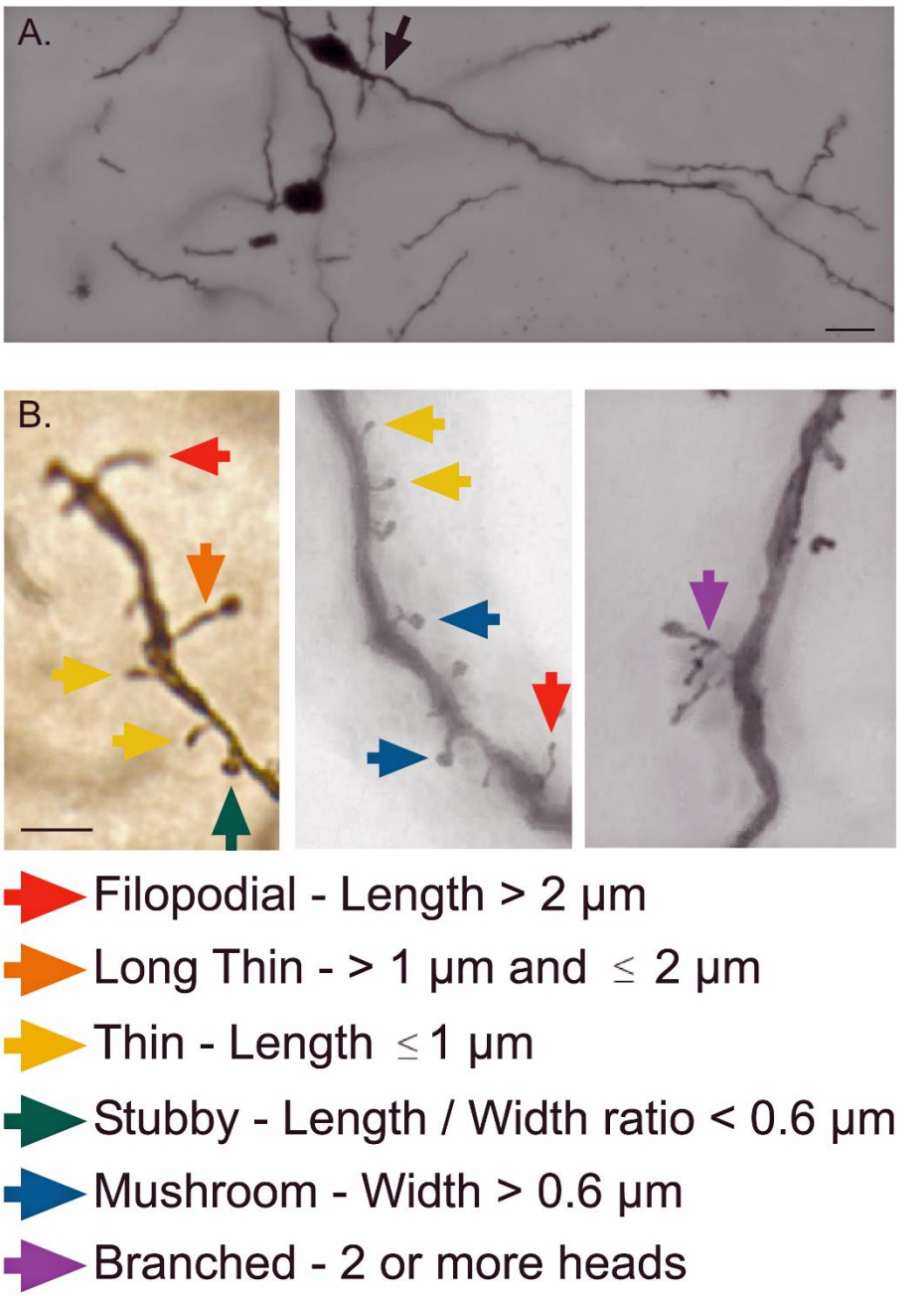
A.
B.
Filopodial - Length > 2 µm
Long Thin - > 1 µm and ≤ 2 µm
Thin - Length ≤ 1 µm
Stubby - Length / Width ratio < 0.6 µm
Mushroom - Width > 0.6 µm
Branched - 2 or more heads

Figure 2:

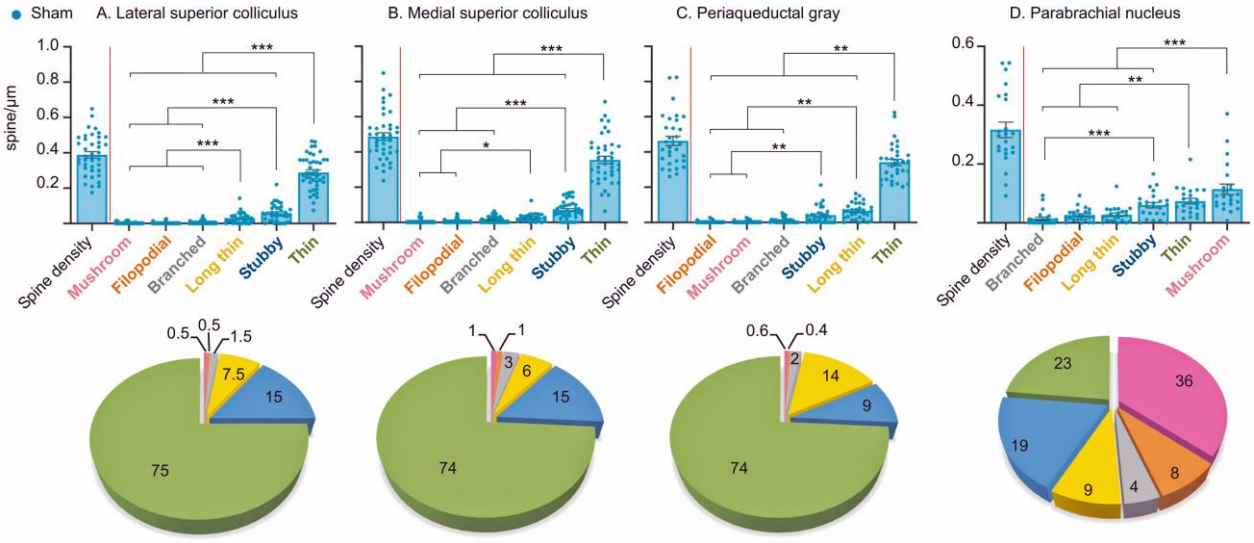
Sham
A. Lateral superior colliculus
B. Medial superior colliculus
C. Periaqueductal gray
D. Parabrachial nucleus
spine/μm
Spine density
Mushroom
Filopodial
Branched
Long thin
Stubby
Thin
0.5
0.5
1.5
7.5
15
75
1
1
3
6
15
74
0.6
0.4
2
14
9
74
23
36
19
9
4
8

Figure 3:

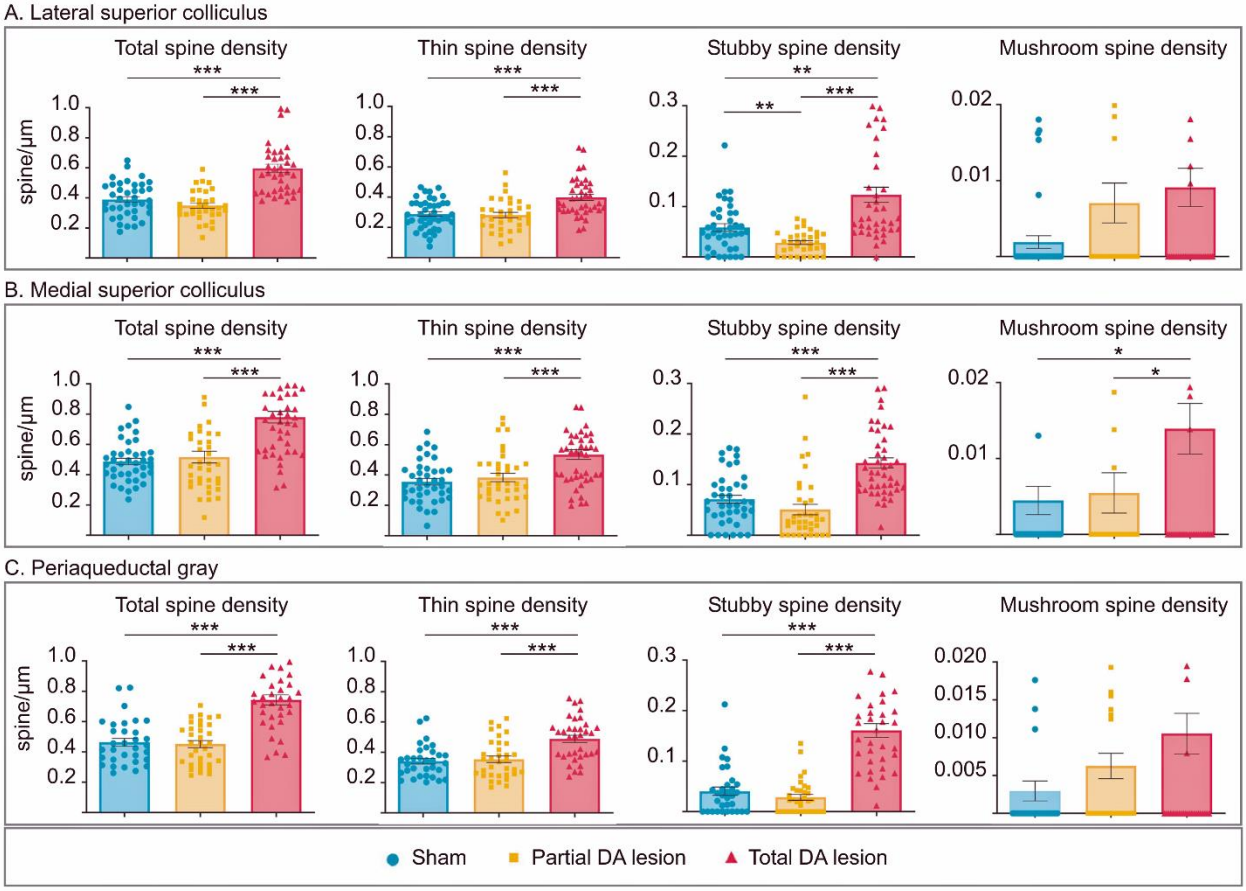
A. Lateral superior colliculus
Total spine density
Thin spine density
Stubby spine density
Mushroom spine density
spine/µm
B. Medial superior colliculus
C. Periaqueductal gray
Sham
Partial DA lesion
Total DA lesion

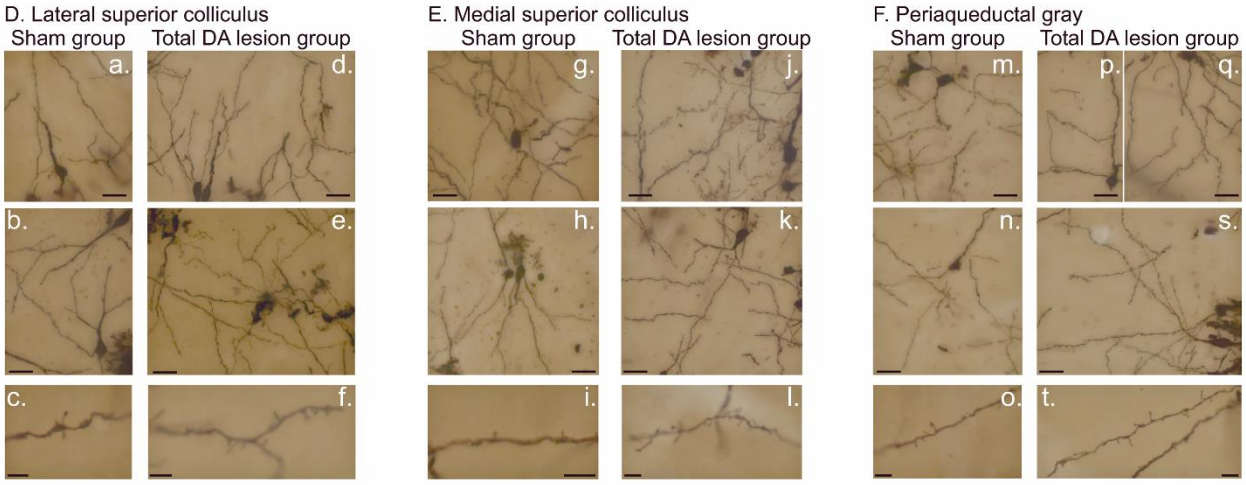
D. Lateral superior colliculus
Sham group
Total DA lesion group
E. Medial superior colliculus
F. Periaqueductal gray

Figure 4:

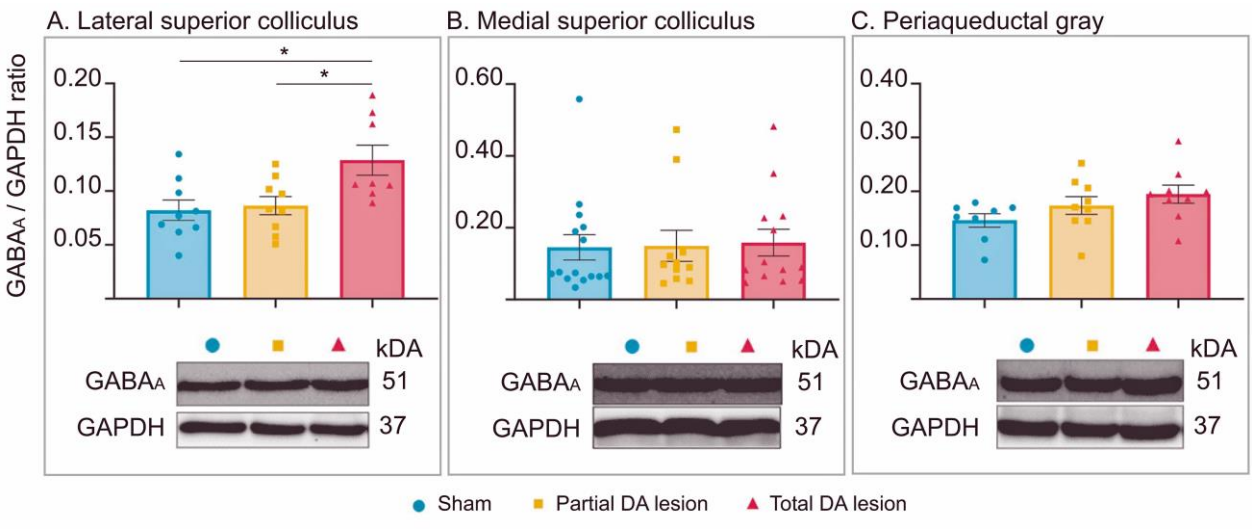
A. Lateral superior colliculus
B. Medial superior colliculus
C. Periaqueductal gray
GABAA / GAPDH ratio
0.20
0.15
0.10
0.05
0.60
0.40
0.20
0.40
0.30
0.20
0.10
*
*
kDA
GABAA
GAPDH
51
37
Sham
Partial DA lesion
Total DA lesion

Table 1:

| **A. Golgi Cox Sham** | | Lateral SC | | | Medial SC | | | PAG | | |
|---|---|---|---|---|---|---|---|---|---|---|
| | Mushroom | 0.0019± 0.0008 | | | 0.0045 ± 0.0018 | | | 0.003 ± 0.0013 | | |
| | Filopodial | 0.002 ± 0.001 | | | 0.0053 ± 0.0019 | | | 0.002 ± 0.001 | | |
| | Branched | 0.0054 ± 0.0017 | | | 0.0157 ± 0.0028 | | | 0.011 ± 0.003 | | |
| | Long thin | 0.0289 ± 0.005 | | | 0.0278 ± 0.0056 | | | 0.065 ± 0.008 | | |
| | Stubby | 0.0586 ± 0.0075 | | | 0.071 ± 0.0081 | | | 0.040 ± 0.008 | | |
| | Thin | 0.289 ± 0.0147 | | | 0.355 ± 0.021 | | | 0.341 ± 0.019 | | |
| | Units | Mean ± SEM - Spines/µm | | | | | | | | |
| | | | | | | | | | | |
| **B. Impact of DA lesion** | | Lateral SC | | | Medial SC | | | PAG | | |
| | | Sham | Partial | Total | Sham | Partial | Total | Sham | Partial | Total |
| Golgi Cox | Density | 0.389 ± 0.018 | 0.3471 ± 0.017 | 0.595 ± 0.0284 | 0.490 ± 0.021 | 0.520 ± 0.0391 | 0.780 ± 0.038 | 0.463 ± 0.0261 | 0.451 ± 0.023 | 0.743 ± 0.0326 |
| | Thin | 0.289 ± 0.0147 | 0.282 ± 0.0177 | 0.398 ± 0.02 | 0.355 ± 0.021 | 0.383 ± 0.028 | 0.535 ± 0.032 | 0.341 ± 0.019 | 0.354 ± 0.022 | 0.490 ± 0.023 |
| | Stubby | 0.0586 ± 0.0075 | 0.0285 ± 0.0038 | 0.123 ± 0.0151 | 0.071 ± 0.0081 | 0.051 ± 0.010 | 0.143 ± 0.010 | 0.040 ± 0.008 | 0.0284 ± 0.006 | 0.160 ± 0.0136 |
| | Mushroom | 0.0019 ± 0.0008 | 0.007 ± 0.0026 | 0.009 ± 0.0025 | 0.0045 ± 0.0018 | 0.0055 ± 0.0026 | 0.014 ± 0.003 | 0.003 ± 0.0013 | 0.006 ± 0.0017 | 0.105 ± 0.0027 |
| | Units | Mean ± SEM - Spines/µm | | | | | | | | |
| | | | | | | | | | | |
| Western blot | $GABA_A$ | 0.082 ± 0.011 | 0.083 ± 0.01 | 0.119 ± 0.011 | 0.14 ± 0.035 | 0.16 ± 0.052 | 0.15 ± 0.032 | 0.156 ± 0.008 | 0.174 ± 0.016 | 0.195 ± 0.017 |
| | Units | GABAA / GAPDH ratio | | | | | | | | |

Supplementary figure 1